Magnetic resonance imaging for lung cancer screen

Yi-Xiang J. Wang[1], Gladys G. Lo[2], Jing Yuan[3], Peder E. Z. Larson[4,5], Xiaoliang Zhang[4,5]

[1]Department of Imaging and Interventional Radiology, Faculty of Medicine, The Chinese University of Hong Kong, Prince of Wales Hospital, Shatin, Hong Kong, China; [2]Department of Diagnostic Radiology, Hong Kong Sanatorium & Hospital, Happy Valley, Hong Kong, China; [3]Medical Physics and Research Department, Hong Kong Sanatorium & Hospital, Happy Valley, Hong Kong, China; [4]Department of Radiology and Biomedical Imaging, University of California San Francisco, San Francisco, CA, USA; [5]UCSF/UC Berkeley Joint Bioengineering Program, San Francisco and Berkeley, CA, USA

Correspondence to: Dr. Yi-Xiang J. Wang. Department of Imaging and Interventional Radiology, Prince of Wales Hospital, The Chinese University of Hong Kong, Shatin, NT, Hong Kong, China. Email: yixiang_wang@cuhk.edu.hk; Dr. Xiaoliang Zhang. Department of Radiology and Biomedical Imaging, University of California San Francisco, San Francisco, CA, USA. Email: xiaoliang.zhang@ucsf.edu.

Abstract: Lung cancer is the leading cause of cancer related death throughout the world. Lung cancer is an example of a disease for which a large percentage of the high-risk population can be easily identified via a smoking history. This has led to the investigation of lung cancer screening with low-dose helical/multi-detector CT. Evidences suggest that early detection of lung cancer allow more timely therapeutic intervention and thus a more favorable prognosis for the patient. The positive relationship of lesion size to likelihood of malignancy has been demonstrated previously, at least 99% of all nodules 4 mm or smaller are benign, while noncalcified nodules larger than 8 mm diameter bear a substantial risk of malignancy. In the recent years, the availability of high-performance gradient systems, in conjunction with phased-array receiver coils and optimized imaging sequences, has made MR imaging of the lung feasible. It can now be assumed a threshold size of 3-4 mm for detection of lung nodules with MRI under the optimal conditions of successful breath-holds with reliable gating or triggering. In these conditions, 90% of all 3-mm nodules can be correctly diagnosed and that nodules 5 mm and larger are detected with 100% sensitivity. Parallel imaging can significantly shorten the imaging acquisition time by utilizing the diversity of sensitivity profile of individual coil elements in multi-channel radiofrequency receive coil arrays or transmit/receive coil arrays to reduce the number of phase encoding steps required in imaging procedure. Compressed sensing technique accelerates imaging acquisition from dramatically undersampled data set by exploiting the sparsity of the images in an appropriate transform domain. With the combined imaging algorithm of parallel imaging and compressed sensing and advanced 32-channel or 64-channel RF hardware, overall imaging acceleration of 20 folds or higher can then be expected, ultimately achieve free-breathing and no ECG gating acquisitions in lung cancer MRI screening. Further development of protocols, more clinical trials and the use of advanced analysis tools will further evaluate the real significance of lung MRI.

Keywords: Lung; cancer; screening; MR; CT

Background of lung cancer screening

Lung cancer is the leading cause of cancer related death throughout the world (1). Lung cancer is also an example of a disease for which a large percentage of the high-risk population can be easily identified via a smoking history. This, coupled with the high success of other screening programs for prostate, breast, and cervical cancers has led to the investigation of lung cancer screening with low-dose multi-detector CT. Evidences suggest that early detection of lung cancer allow more timely therapeutic intervention and thus a more favorable prognosis for the patient (2-4).

The majority of smokers who undergo thin-section CT have been found to have small lung nodules, most of which

are smaller than 7 mm in diameter (5,6). However, nodule features such as shape, edge characteristics, cavitation, and location have not yet been found to be accurate for distinguishing benign from malignant nodules (7,8). The positive relationship of lesion size to likelihood of malignancy has been clearly demonstrated (9-12). In a meta-analysis of eight large screening trials, the prevalence of malignancy depended on the size of the nodules, ranging from 0% to 1% for nodules 5 mm or smaller, 6% to 28% for those between 5 and 10 mm, and 64% to 82% for nodules 20 mm or larger (9). Even in smokers, the percentage of all nodules smaller than 4 mm that will eventually turn into lethal cancers is very low (<1%), whereas for those in the 8-mm range the percentage is approximately 10-20%. The 2005 Fleischner Society guideline stated that at least 99% of all nodules 4 mm or smaller are benign and because such small opacities are common on thin-section CT scans, follow-up CT in every such case is not recommended; in selected cases with suspicious morphology or in high-risk subjects, a single follow-up scan in 12 months should be considered (13).

When the nodule is 5-9 mm in diameter, approximately 6% of cases showed interval nodule growth detectable on 4-8 month follow-up scans (10). For these nodules the best strategy is regular follow-up. The timing of these control examinations varies according to the nodule size (4-6, or 6-8 mm) and type of patients, specifically at low or high risk of malignancy concerned. Frequent follow-up increases radiation burden for the affected population (14-16). The radiation dosage for a chest varies between 1-10 mSv, while that of whole body FDG-PET/CT is 10-30 mSv. More details on medical X-ray radiation risk can be found at (http://www.xrayrisk.com/).

Noncalcified nodules larger than 8 mm diameter can bear a substantial risk of malignancy (9,12,13). In the case of nodules larger than 8 mm, additional options such as contrast material-enhanced CT, positron emission tomography (PET), percutaneous needle biopsy, and thoracoscopic resection or video-assisted thoracoscopic can be considered (9,17).

Current status of MR imaging for the lung

Use of MRI in the evaluation of pulmonary nodules has thus far been limited. The reasons include limited spatial resolution, high susceptibility differences between air spaces and pulmonary interstitium, and the presence of respiratory and cardiac motion artifacts. However, in the recent years, the availability of high-performance gradient systems, in conjunction with phased-array receiver coils and optimized imaging sequences, has made new approaches possible to MR-based pulmonary imaging (*Figures 1,2*). Electrocardiogram (ECG) and respiratory triggering or breath-holding techniques is used to eliminate the motion artifacts.

Turbo spine echo sequence shows many pulmonary nodules, including lung cancers, pulmonary metastases, and low-grade malignancies such as carcinoids and lymphomas, with low- or intermediate-signal intensity on T1-weighted imaging and slightly high intensity on T2-weighted imaging (18). For various pulmonary metastasizing malignancies, with a 1.5 T scanner and breath-hold 2D Half-Fourier Acquisition Single-Shot Turbo Spin-Echo (HASTE) sequence Schroeder *et al.* (19) reported an axial spatial resolution of 2.4×1.3 mm^2. To compensate for the poor resolution in the z-axis of slice thickness of 5 mm, image sets in both the axial and coronal planes were collected (19). The sensitivity values for the HASTE MR sequence were 73% for lesions smaller than 3 mm, 86.3% for lesions between 3 and 5 mm, 95.7% for lesions between 6 and 10 mm, and 100% for lesions bigger than 10 mm. Although the spatial resolution of the HASTE MR sequence is lower than that of multi-detector CT, both imaging techniques correlated well regarding the determination of size, number, and location of the pulmonary lesions. Pulmonary arteries and veins are depicted as flow voids without any apparent signal black blood inversion sequence. This represents an advantage over CT, on which small pulmonary masses often have attenuation levels similar to those of blood vessels and thus are often indistinguishable from vessels of similar size. Recently, Koyama *et al.* (20) directly compared capabilities of pulmonary nodule detection and differentiation of malignant from benign nodules between noncontrast-enhanced multi-detector CT and MRI using a 1.5 T system in 161 patients with 200 pulmonary nodules. Although the overall detection rate of thin-section multi-detector CT was superior to that of respiratory-triggered short tau inversion recovery (STIR) turbo SE imaging, there were no significant differences in malignant nodule detection rate between the methods (20). In that study the malignant nodule detection rate including bronchioalveolar carcinoma had no significant difference between thin-section multi-detector CT and noncontrast-enhanced MRI, but significantly more benign nodules were missed on noncontrast-enhanced MRI. Koyama *et al.* suggested that it would be preferable to accept a decrease in the detection
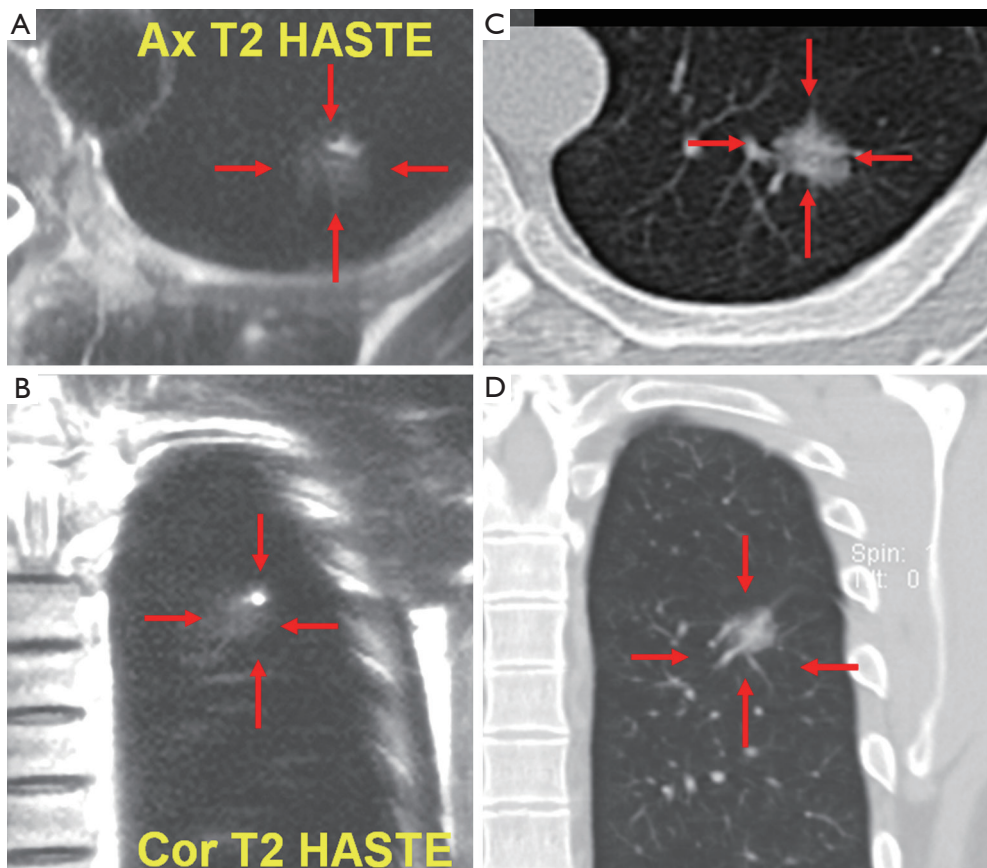
1342

Wang et al. Lung cancer screening using MRI

Figure 1 A 42-year-old male. T2 weighted HASTE MR axial (A) and coronal (B) imaging of the chest shows a nodule (arrows). It was also shown by CT (C, axial; D, coronal) and confirmed to be a bronchioalveolar carcinoma by surgery. HASTE, Half-Fourier Acquisition Single-Shot Turbo Spin-Echo.
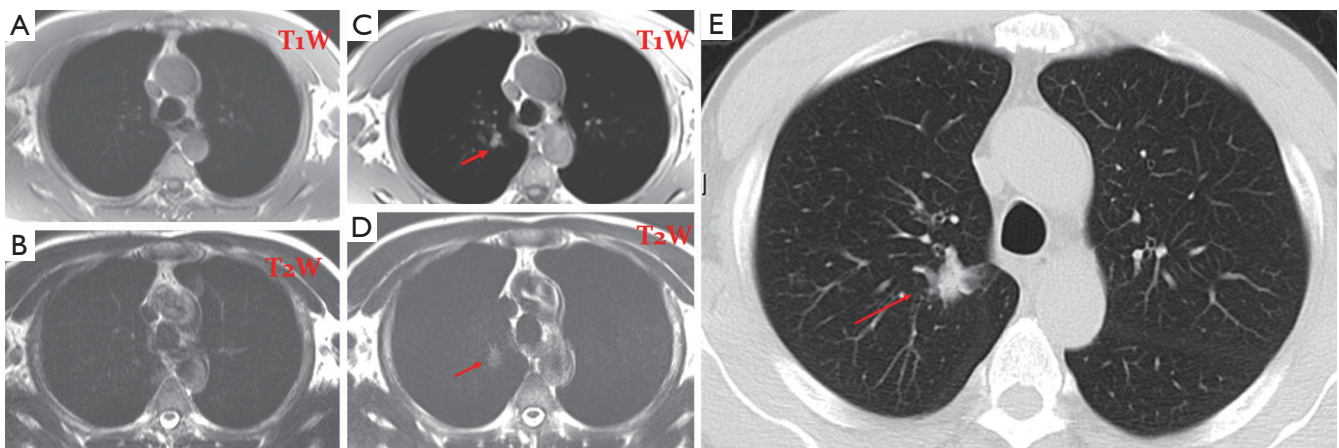

Figure 2 A 72-year-old male. (A,B) T1 & T2 weighted MR screening of the chest; no abnormality was detected in 2005; (C,D) T1 & T2 weighted MR screening of the chest shows a nodule (arrow) in 2008. It was also shown by CT (E) and confirmed to be a bronchioalveolar carcinoma (stage I) by surgery.
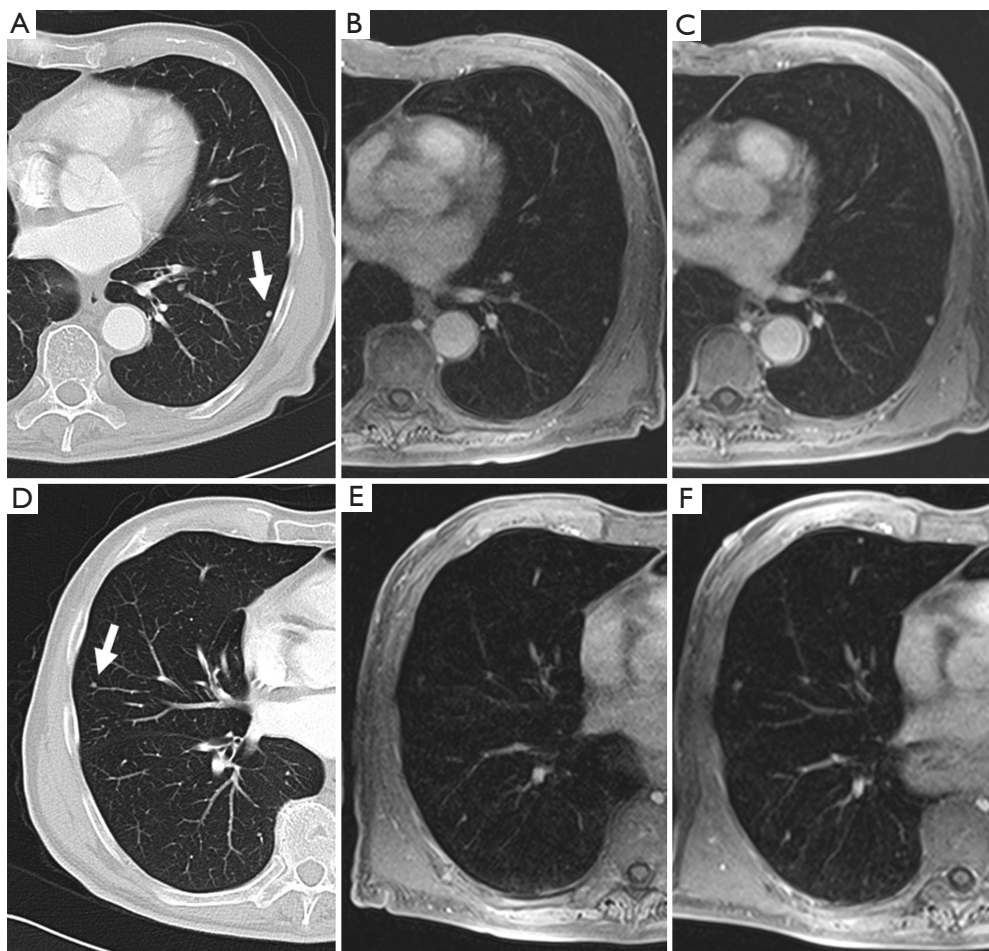
Figure 3 An example demonstrates MRI for the detection of small lung nodules: (A,D) small pulmonary metastases of a malignant melanoma in a 62-year-old patient (5 mm slices of a standard helical CT scan); (B,E) MRI of the corresponding positions at the same time; (C,E) the follow-up MRI after 3 months [the contrast enhanced transverse 3D-GRE (VIBE) images; TR/TE 3.15/1.38 ms, flip angle 8°, FOV 350 mm × 400 mm, slice thickness 4 mm]. The clearly visible 3 mm nodule in the left lower lobe [(A) and (B); marked with an arrow on (A)] grew to a diameter of 5 mm within 3 months (C). Another 3 mm nodule in the lateral right middle lobe [marked with an arrow on (D)] is hardly visible on the corresponding MRI due to cardiac pulsation, but becomes clearer in the follow up study after growing to 4-5 mm (F) [Reproduced with permission from reference (23)].

rate of benign nodules without significantly missing malignant nodules (20).

Studies have shown that 3-T systems afford higher lesion contrast, higher spatial resolution, and less image blurring with shorter echo trains at high acceleration factors than do 1.5-T systems (21). 3D or 2D gradient recalled echo (GRE) and T2-weighted fast spin-echo or T2-weighted HASTE sequences are practical for detection of pulmonary nodules. Puderbach et al. (22) suggested detailed standard protocols for lung MRI, including a transverse T1-weighted breath-hold 3D-GRE sequence and a breath-hold coronal T2-weighted HASTE sequence. It can now be assumed a

threshold size of 3-4 mm for detection of lung nodules with MRI under the optimal conditions of successful breath-holds with reliable gating or triggering. Biederer et al. (23) suggested that 90% of all 3-mm nodules are correctly diagnosed and that nodules 5 mm and larger are detected with 100% sensitivity (*Figure 3*).

While in view of the limited spatial resolution of MR imaging, MRI's differentiation on morphologic criteria is not likely to be better than CT, however, the analysis of signal properties or enhancement profiles may aid in this regard. For example, because MRI affords better tissue contrast, MRI with thin-slice collimation of a pulmonary
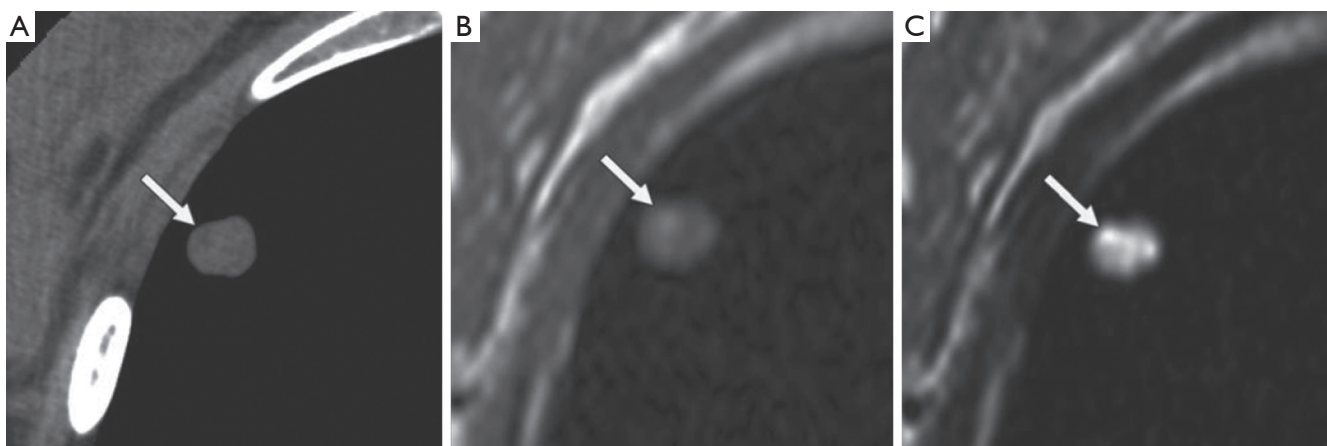
1344

Wang et al. Lung cancer screening using MRI

Figure 4 A 40-year-old woman with pulmonary hamartoma. (A) CT image shows low-attenuation spot (arrow) within nodule, suggesting lipoid tissue; (B,C) axial T1-weighted (B) and T2-weighted (C) MR images show hyperintense spots (arrows) within nodule. T2-weighted image (C) also shows hyper-intense matrix consistent with cartilaginous tissue [Reproduced with permission from reference (21)].

hamartoma shows the fat and calcification foci and can be interpreted in a manner similar to that for CT (*Figure 4*). Fat suppression techniques are also preferable when macroscopic fat is suspected. Chemical-shift MRI with in- and opposed-phase acquisition may be an important tool for detecting fat in pulmonary hamartomas (24). In the absence of markedly calcified cartilaginous tissue, myxoid matrices of the cartilaginous tissue produce very high signal intensity on T2-weighted images (25). Although MRI detection of pulmonary nodules is inferior to CT detection, MRI yields supplementary morphologic information that is valuable for differential diagnosis, including for sclerosing hemangioma, bronchial carcinoid tumor, tuberculoma, aspergillosis, progressive massive fibrosis (21).

Enhancement patterns or blood supply evaluated with dynamic contrast-enhanced (CE) MRI is helpful for diagnosis of pulmonary nodules (26,27). It has been suggested that dynamic CE MRI is effective for assessment of tumor angiogenesis (27). The lack of ionizing radiation makes MRI a safe tool for repeated dynamic evaluations of tumor perfusion. Dynamic MRI with the 3D GRE sequence requires less than 30 second breath-holding for acquisition of all data (26). There are various dynamic MR techniques for distinguishing malignant nodules from benign nodules, with reported sensitivities range from 94-100%, specificities from 70-96%, and accuracies of more than 94% (28-30). These specificities and accuracies for dynamic MRI are equal to those for FDG-PET or PET/CT (27). A recent meta-analysis reported that there were no significant differences in diagnostic performance among

dynamic CE-CT, dynamic CE-MRI, FDG-PET and single photon emission tomography (SPECT) (31).

Recently, diffusion-weighted imaging (DWI) has been suggested as new method for nodule detection and/or evaluation including subtype classification of pulmonary adenocarcinoma (28,29,32). Theoretically, DWI, as does the apparent diffusion coefficient (ADC), assesses the diffusivity of water molecules within tissue in terms of cellularity, perfusion, tissue disorganization, extracellular space, and other variables (28). Quantitative and/or qualitative sensitivities and specificities of the ADC for differentiation of malignant from benign SPNs were 70.0% to 88.9% for sensitivity and 61.1% to 97.0% for specificity (28,30,32). One report stated specificity of DWI (97.0%) was higher than that of FDG-PET/CT (79.0%) (28).

The direct multiplanar capability of MRI is also one of the advantages for the detection of lymph nodes in areas that are suboptimally imaged in the axial plane, such as in the aortopulmonary window and subcarinal regions. Nowadays whole-body MRI has become clinically feasible with the installation of fast imaging and moving table equipment. Whole body DWI has been recommended as a promising new tool for whole-body MR examination of oncologic patients (33-39). When comparing whole-body MRI with FDG-PET for the M-classification capability of head and neck metastases, including brain metastases, the accuracy (80.0%) of whole-body MRI was significantly better than that of FDG-PET (73.3%). When this technique adapted for M-stage assessment including brain metastasis in non-small-cell lung carcinoma, diagnostic accuracy of

whole-body MRI with DW imaging (87.7%) showed no significant difference with that of integrated FDG-PET/CT (88.2%) on a per patient basis (40). Early ADC changes observed after the initial chemotherapy course reportedly correlated with the final tumor size reduction (41).

Computer assisted detection and diagnosis (CAD) systems are becoming increasingly important in the clinical setting, serving as a second reader in image interpretation, effectively improving the detection accuracy and consistency of pulmonary nodules in chest X-ray and CT (42). Awai *et al.* (43) compared the nodule detecting performance of five radiologists and five radiology residents in 50 chest CT scans. Statistically significant improvements in lung nodule detection were achieved for all radiologists using the CAD system (P<0.1), with a true positive rate of 94%. The CAD for MRI has not yet been developed. The development of CAD for MRI can be greatly assisted by the techniques already established for CT.

In the meantime, it is important to note that the clinical importance of detecting a 3 mm nodule in a patient with malignant disease and the decisions for treatment depending on the absence of lung metastases differs from detecting a similar lesion in a healthy patient who takes part in a screening program. In a patient with known primary malignancy lung nodules would be deemed suspicious for metastases (9). MRI cannot replace CT for the diagnosis of pulmonary metastases (21). Although 6-mm or greater-diameter pulmonary metastatic nodules may be readily identified with MRI, smaller nodules in lung (<6 mm) are detected with less sensitivity (34,44).

Future directions of MR technology development for lung cancer screening

Current MRI techniques are capable of detecting 4 mm or larger nodules with reasonable spatial resolution and provide clinically valuable information for prognosis and management of possible lung cancers. Till now the imaging acquisition is usually performed with breath-holding and/or some gating methods to reduce motion artifacts caused by respiratory motion, heart beating and cerebrospinal fluid pulsation. The current imaging protocols for lung cancer imaging have a total acquisition time of ~20 seconds for a single scan. Twenty-second breath-holding is often challenging for patients, and long breath-holding increases the possibility of inducing involuntary motions during the imaging acquisition. It is desired to have a much faster imaging method to image the lung so that respiratory and

ECG gating can be eliminated in the lung cancer imaging protocols.

The use of high field MR scanner improves the sensitivity and provides more signals for expediting image acquisition. Recent advance in fast MR imaging using parallel imaging and compressed sensing technology have made a great impact in MR imaging community and demonstrated excellent capability in accelerating MR imaging acquisition (45-48). Parallel imaging can significantly shorten the imaging acquisition time by utilizing the diversity of sensitivity profile of individual coil elements in multi-channel radiofrequency receive coil arrays or transmit/receive coil arrays to reduce the number of phase encoding steps required in imaging procedure (49-52). The performance of multi-channel radiofrequency coil arrays is critical to parallel imaging and its imaging acceleration capability (53-56). Unlike parallel imaging techniques, recently introduced compressed sensing technique accelerates imaging acquisition from dramatically undersampled data set by exploiting the sparsity of the images in an appropriate transform domain (4,57-59). Compressed sensing technique can be implemented by using not only multi-channel radiofrequency coil arrays but also conventional non-array radiofrequency coils. Given large field-of-view requirement in lung imaging and currently radiofrequency coil array technology, it is technically challenging to accelerate the imaging by 20-fold or more and make lung imaging acquisition time down to 5 second or less by using parallel imaging technique or compressed sensing technique alone. To achieve this goal, a technique that combines parallel imaging and compressed sensing with optimized imaging parameters and acceleration performance has to be developed. In addition, an advanced multi-channel (e.g., 32-channel, or 64-channel) radiofrequency coil array for lung imaging with sufficient imaging coverage, MR sensitivity and parallel imaging performance is also needed. A major challenge in the design of radiofrequency coil arrays with large channel counts is the electromagnetic coupling among the channels or array elements. This most likely can be addressed by using recently introduced magnetic wall or induced current compensation or elimination (ICE) decoupling technique which has demonstrated a unique capability in decoupling densely-placed resonant elements in massive arrays (60). For a 32-channel or 64-channel RF coil array, it is possible to accelerate imaging by 5-6 folds based on parallel imaging technique with no noticeable image artifacts or distortion. On the top of this, further acceleration of 4 folds can be

1346

Wang et al. Lung cancer screening using MRI

obtained by using compressed sensing technique or its derivatives, given the good sparsity behavior of lung images. Therefore, with the combined imaging algorithm of parallel imaging and compressed sensing and advanced 32-channel or 64-channel RF hardware, overall imaging acceleration of 20 folds or higher can then be expected. This could reduce the acquisition time of lung imaging protocols down to 5 second or less, ultimately achieving free-breathing and no ECG gating acquisitions in lung cancer MRI screening.

Another promising technique for imaging pulmonary nodules is ultrashort echo time (UTE) MR image. This technique uses specialized radiofrequency excitation pulses with center-out k-space trajectories to minimize the echo time (61). This ultimately allows for direct imaging of the lung parenchyma, which has a T2 of ~80 ms T2* of ~0.5-3 ms due to the high susceptibility. UTE MR imaging is also advantageous for lung imaging because it is relatively robust to motion artifacts and therefore high quality clinical images can be acquired with free-breathing in the limited field-of-view setting despite the regular non-accelerated acquisitions (62). Recent preclinical studies have shown excellent results depicting lung cancer nodules in a mouse model even without cardiac or respiratory gating (63).

Conclusions

The current development in MR technology data are encouraging for considering follow-up studies of proven pulmonary cancer and for pulmonary screening of populations at risk for pulmonary cancer. Whole body MR screening has also become a reality. Further development of protocols, more clinical trials and advanced analysis tools will further evaluate the real significance of lung MRI.

Acknowledgements

References

1. Ferlay J, Shin HR, Bray F, et al. Estimates of worldwide burden of cancer in 2008: GLOBOCAN 2008. Int J Cancer 2010;127:2893-917.
2. Sone S, Takashima S, Li F, et al. Mass screening for lung cancer with mobile spiral computed tomography scanner. Lancet 1998;351:1242-5.
3. Heelan RT, Flehinger BJ, Melamed MR, et al. Non-small-cell lung cancer: results of the New York screening program. Radiology 1984;151:289-93.
4. National Lung Screening Trial Research Team, Aberle DR, Adams AM, et al. Reduced lung-cancer mortality with low-dose computed tomographic screening. N Engl J Med 2011;365:395-409.
5. Swensen SJ, Silverstein MD, Ilstrup DM, et al. The probability of malignancy in solitary pulmonary nodules. Application to small radiologically indeterminate nodules. Arch Intern Med 1997;157:849-55.
6. Swensen SJ. CT screening for lung cancer. AJR Am J Roentgenol 2002;179:833-6.
7. Brandman S, Ko JP. Pulmonary nodule detection, characterization, and management with multidetector computed tomography. J Thorac Imaging 2011;26:90-105.
8. Zhao F, Yan SX, Wang GF, et al. CT features of focal organizing pneumonia: an analysis of consecutive histopathologically confirmed 45 cases. Eur J Radiol 2014;83:73-8.
9. Wang YX, Gong JS, Suzuki K, et al. Evidence based imaging strategies for solitary pulmonary nodule. J Thorac Dis 2014;6:872-87.
10. Henschke CI, Yankelevitz DF, Naidich DP, et al. CT screening for lung cancer: suspiciousness of nodules according to size on baseline scans. Radiology 2004;231:164-8.
11. Swensen SJ, Jett JR, Hartman TE, et al. Lung cancer screening with CT: Mayo Clinic experience. Radiology 2003;226:756-61.
12. Henschke CI, Naidich DP, Yankelevitz DF, et al. Early lung cancer action project: initial findings on repeat screenings. Cancer 2001;92:153-9.
13. MacMahon H, Austin JH, Gamsu G, et al. Guidelines for management of small pulmonary nodules detected on CT scans: a statement from the Fleischner Society. Radiology 2005;237:395-400.
14. Mayo JR, Aldrich J, Muller NL, et al. Radiation exposure at chest CT: a statement of the Fleischner Society. Radiology 2003;228:15-21.
15. Imhof H, Schibany N, Ba-Ssalamah A, et al. Spiral CT and radiation dose. Eur J Radiol 2003;47:29-37.
16. Brenner DJ. Radiation risks potentially associated with low-dose CT screening of adult smokers for lung cancer. Radiology 2004;231:440-5.
17. Sim YT, Poon FW. Imaging of solitary pulmonary nodule-a clinical review. Quant Imaging Med Surg 2013;3:316-26.
18. Koyama H, Ohno Y, Seki S, et al. Magnetic resonance imaging for lung cancer. J Thorac Imaging 2013;28:138-50.

19. Schroeder T, Ruehm SG, Debatin JF, et al. Detection of pulmonary nodules using a 2D HASTE MR sequence: comparison with MDCT. AJR Am J Roentgenol 2005;185:979-84.

20. Koyama H, Ohno Y, Kono A, et al. Quantitative and qualitative assessment of non-contrast-enhanced pulmonary MR imaging for management of pulmonary nodules in 161 subjects. Eur Radiol 2008;18:2120-31.

21. Kurihara Y, Matsuoka S, Yamashiro T, et al. MRI of pulmonary nodules. AJR Am J Roentgenol 2014;202:W210-6.

22. Puderbach M, Hintze C, Ley S, et al. MR imaging of the chest: a practical approach at 1.5T. Eur J Radiol 2007;64:345-55.

23. Biederer J, Hintze C, Fabel M. MRI of pulmonary nodules: technique and diagnostic value. Cancer Imaging 2008;8:125-30.

24. Hochhegger B, Marchiori E, dos Reis DQ, et al. Chemical-shift MRI of pulmonary hamartomas: initial experience using a modified technique to assess nodule fat. AJR Am J Roentgenol 2012;199:W331-4.

25. Sakai F, Sone S, Kiyono K, et al. MR of pulmonary hamartoma: pathologic correlation. J Thorac Imaging 1994;9:51-5.

26. Kono R, Fujimoto K, Terasaki H, et al. Dynamic MRI of solitary pulmonary nodules: comparison of enhancement patterns of malignant and benign small peripheral lung lesions. AJR Am J Roentgenol 2007;188:26-36.

27. Fujimoto K, Abe T, Müller NL, et al. Small peripheral pulmonary carcinomas evaluated with dynamic MR imaging: correlation with tumor vascularity and prognosis. Radiology 2003;227:786-93.

28. Uto T, Takehara Y, Nakamura Y, et al. Higher sensitivity and specificity for diffusion-weighted imaging of malignant lung lesions without apparent diffusion coefficient quantification. Radiology 2009;252:247-54.

29. Koyama H, Ohno Y, Aoyama N, et al. Comparison of STIR turbo SE imaging and diffusion-weighted imaging of the lung: capability for detection and subtype classification of pulmonary adenocarcinomas. Eur Radiol 2010;20:790-800.

30. Mori T, Nomori H, Ikeda K, et al. Diffusion-weighted magnetic resonance imaging for diagnosing malignant pulmonary nodules/masses: comparison with positron emission tomography. J Thorac Oncol 2008;3:358-64.

31. Cronin P, Dwamena BA, Kelly AM, et al. Solitary pulmonary nodules: meta-analytic comparison of cross-sectional imaging modalities for diagnosis of malignancy. Radiology 2008;246:772-82.

32. Satoh S, Kitazume Y, Ohdama S, et al. Can malignant and benign pulmonary nodules be differentiated with diffusion-weighted MRI? AJR Am J Roentgenol 2008;191:464-70.

33. Wilhelm T, Stieltjes B, Schlemmer HP. Whole-body-MR-diffusion weighted imaging in oncology. Rofo 2013;185:950-8.

34. Lauenstein TC, Goehde SC, Herborn CU, et al. Whole-body MR imaging: evaluation of patients for metastases. Radiology 2004;233:139-48.

35. Charles-Edwards EM, deSouza NM. Diffusion-weighted magnetic resonance imaging and its application to cancer. Cancer Imaging 2006;6:135-43.

36. Ohno Y, Koyama H, Nogami M, et al. Whole-body MR imaging vs. FDG-PET: comparison of accuracy of M-stage diagnosis for lung cancer patients. J Magn Reson Imaging 2007;26:498-509.

37. Ohno Y, Koyama H, Nogami M, et al. STIR turbo SE MR imaging vs. coregistered FDG-PET/CT: quantitative and qualitative assessment of N-stage in non-small-cell lung cancer patients. J Magn Reson Imaging 2007;26:1071-80.

38. Ciliberto M, Maggi F, Treglia G, et al. Comparison between whole-body MRI and Fluorine-18-Fluorodeoxyglucose PET or PET/CT in oncology: a systematic review. Radiol Oncol 2013;47:206-18.

39. Lo GG, Ai V, Au-Yeung KM, et al. Magnetic resonance whole body imaging at 3 Tesla: feasibility and findings in a cohort of asymptomatic medical doctors. Hong Kong Med J 2008;14:90-6.

40. Ohno Y, Koyama H, Onishi Y, et al. Non-small cell lung cancer: whole-body MR examination for M-stage assessment--utility for whole-body diffusion-weighted imaging compared with integrated FDG PET/CT. Radiology 2008;248:643-54.

41. Yabuuchi H, Hatakenaka M, Takayama K, et al. Non-small cell lung cancer: detection of early response to chemotherapy by using contrast-enhanced dynamic and diffusion-weighted MR imaging. Radiology 2011;261:598-604.

42. Suzuki K. A review of computer-aided diagnosis in thoracic and colonic imaging. Quant Imaging Med Surg 2012;2:163-76.

43. Awai K, Murao K, Ozawa A, et al. Pulmonary nodules at chest CT: effect of computer-aided diagnosis on radiologists' detection performance. Radiology 2004;230:347-52.

44. Platzek I, Zastrow S, Deppe PE, et al. Whole-body MRI in follow-up of patients with renal cell carcinoma. Acta Radiol 2010;51:581-9.

1348

Wang et al. Lung cancer screening using MRI

45. Sodickson DK, Manning WJ. Simultaneous acquisition of spatial harmonics (SMASH): fast imaging with radiofrequency coil arrays. Magn Reson Med 1997;38:591-603.

46. Pruessmann KP, Weiger M, Scheidegger MB, et al. SENSE: sensitivity encoding for fast MRI. Magn Reson Med 1999;42:952-62.

47. Griswold MA, Jakob PM, Heidemann RM, et al. Generalized autocalibrating partially parallel acquisitions (GRAPPA). Magn Reson Med 2002;47:1202-10.

48. Lustig M, Donoho D, Pauly JM. Sparse MRI: The application of compressed sensing for rapid MR imaging. Magn Reson Med 2007;58:1182-95.

49. Pang Y, Vigneron DB, Zhang X. Parallel traveling-wave MRI: a feasibility study. Magn Reson Med 2012;67:965-78.

50. Pang Y, Wong EW, Yu B, et al. Design and numerical evaluation of a volume coil array for parallel MR imaging at ultrahigh fields. Quant Imaging Med Surg 2014;4:50-6.

51. Kurpad KN, Boskamp EB, Wright SM. Eight channel transmit array volume coil using on-coil radiofrequency current sources. Quant Imaging Med Surg 2014;4:71-8.

52. Pang Y, Yu B, Vigneron DB, et al. Quadrature transmit array design using single-feed circularly polarized patch antenna for parallel transmission in MR imaging. Quant Imaging Med Surg 2014;4:11-8.

53. Wang C, Li Y, Wu B, et al. A practical multinuclear transceiver volume coil for in vivo MRI/MRS at 7 T. Magn Reson Imaging 2012;30:78-84.

54. Li Y, Pang Y, Vigneron D, et al. Investigation of multichannel phased array performance for fetal MR

imaging on 1.5T clinical MR system. Quant Imaging Med Surg 2011;1:24-30.

55. Geethanath S, Reddy R, Konar AS, et al. Compressed sensing MRI: a review. Crit Rev Biomed Eng 2013;41:183-204.

56. Hu X, Chen X, Liu X, et al. Parallel imaging performance investigation of an 8-channel common-mode differential-mode (CMDM) planar array for 7T MRI. Quant Imaging Med Surg 2014;4:33-42.

57. Chang CH, Ji JX. Improving multi-channel compressed sensing MRI with reweighted l 1 minimization. Quant Imaging Med Surg 2014;4:19-23.

58. Liang D, Liu B, Ying L. Accelerating sensitivity encoding using compressed sensing. Conf Proc IEEE Eng Med Biol Soc 2008;2008:1667-70.

59. Pang Y, Yu B, Zhang X. Enhancement of the low resolution image quality using randomly sampled data for multi-slice MR imaging. Quant Imaging Med Surg 2014;4:136-44.

60. Li Y, Xie Z, Pang Y, et al. ICE decoupling technique for RF coil array designs. Med Phys 2011;38:4086-93.

61. Bergin CJ, Pauly JM, Macovski A. Lung parenchyma: projection reconstruction MR imaging. Radiology 1991;179:777-81.

62. Johnson KM, Fain SB, Schiebler ML, et al. Optimized 3D ultrashort echo time pulmonary MRI. Magn Reson Med 2013;70:1241-50.

63. Bianchi A, Dufort S, Fortin PY, et al. In vivo MRI for effective non-invasive detection and follow-up of an orthotopic mouse model of lung cancer. NMR Biomed 2014;27:971-9.